Hydrol. Earth Syst. Sci. Discuss., 8, 7055–7090, 2011
www.hydrol-earth-syst-sci-discuss.net/8/7055/2011/
doi:10.5194/hessd-8-7055-2011

Hydrology and Earth System Sciences Discussions

Physically-based modeling of topographic effects on spatial evapotranspiration and soil moisture patterns in complex terrain

M. Liu[1,2], A. Bárdossy[3], J. Li[3], and Y. Jiang[1]

[1]State Key Laboratory of Earth Surface Processes and Resource Ecology, Beijing Normal University, Beijing, China
[2]Helmholtz Research Centre for Environment, Magdeburg, Germany
[3]Institute of Hydraulic Engineering, University of Stuttgart, Stuttgart, Germany

Received: 23 June 2011 – Accepted: 4 July 2011 – Published: 20 July 2011

Correspondence to: M. Liu (min.liu@iws.uni-stuttgart.de)

Published by Copernicus Publications on behalf of the European Geosciences Union.

Abstract

Simulation with the Soil Water Atmosphere Plant (SWAP) model is performed to quantify the spatial variability of evapotranspiration (ET) and soil moisture content (SMC) caused by topography-induced spatial wind and radiation differences. The field scale SWAP model is applied in a distributed way, i.e. for each grid, assuming linear groundwater table, identical boundary conditions and no lateral flow. Input of spatial wind and solar radiation are obtained with the adapted *r.sun* model and the meso-scale METRAS PC model based on physical mechanisms respectively. Both potential and actual ET, as well as the individual components of evaporation and transpiration are calculated by the model. The numerical experiments are conducted for grids at two different resolutions (100 m and 1000 m) to evaluate the scale effects. At fine scale, both solar radiation and wind have a strong effect on spatial ET/SMC pattern, whereas at coarse scale, the wind effect dominates. The results show a strong spatial and temporal intra-catchment variability in daily/annual total ET and less variability in soil moisture. The spatial variability in ET is associated with a difference in total amount of runoff generated, which may lead to a significant consequence in catchment water balance, snowmelt and rainfall-runoff generation processes.

1 Introduction

Evapotranspiration is a very important element in hydrological cycle, and it is adopted as the criteria for climate classification (Thornthwaite and Mather, 1955). Globally evapotranspiration amounts to more than 60 % of the precipitation that falls on the continents (Dingman, 2002), and in arid and semi-arid regions it is much higher. At long-term, evapotranspiration determines the regional water balance and hydro-ecological system, whereas at short-term, it affects the crop growth and yield, as well as the antecedent moisture conditions (AMC) which controls the rainfall-runoff generation processes from the nearest meteorological station, thus the hydrologic response of an area. The importance of ET and SMC is manifested both on small agriculture field scale and in large-scale modelling of land atmosphere interaction. For most climate conditions, soil moisture and evapotranspiration are strongly coupled together, and they are the key parameters for soil water budget, which helps to optimize water balance management and forecast the flash floods (Cassardo et al., 2002; Norbiato et al., 2008). Temporal ET and SMC dynamics also has a strong implication on the interpretation of global climate change.

Several characteristic ET values are available in the literatures, i.e. potential ET (ETP), actual ET (ETA), and reference ET. PET is originally defined as "the amount of water transpired in a given time by a short green crop, completely shading the ground, of uniform height and with adequate water status in the soil profile" by Penman (1948), and it has been generalized to describe the maximum evapotranspiration possible under specific climatic conditions with unlimited water availability in the soil for any vegetation. ETA is the exact water loss by soil and vegetation under water stress conditions. Reference ET is the definition adopted by FAO (1990), which refers to "the rate of evapotranspiration from a hypothetical reference crop with an assumed crop height of 0.12 m, a fixed surface resistance of 70 $\mathrm{sec\,m^{-1}}$ and an albedo of 0.23, closely resembling the evapotranspiration from an extensive surface of green grass of uniform height, actively growing, well-watered and completely shading the ground". In this work, the terms of ETP in general sense and ETA are used.

ET/SMC show a high spatial heterogeneity at different scales (Bresnahan and Miller, 1997; Western et al., 2002), resulted from the interaction of local atmospheric factors (precipitation, radiation, temperature, humidity, pressure, etc.), soil characteristics and vegetation covers, all of which possess a highly heterogeneous nature and many of which show a dependence on topography. Except radiation, wind and temperature, for most of these factors, such as soil texture and vegetation features, it is difficult to quantify their spatial distribution with topography. But this does not contradict to the fact that, topography plays an important role in the spatial distribution of ET/SMC. The

HESSD
8, 7055–7090, 2011

spatial pattern of ET/SMC gives insight into the spatial water consumption, provides necessary information for water resource allocation and land use management and helps to understand the spatial rainfall-runoff generation processes. Understanding, monitoring and quantifying the spatial ET/SMC variability as well as the topographic effects on these variability is important for both theoretical and practical purpose in catchment hydrology.

In contrast to other hydrological parameters such as precipitation and temperature, reliable direct measurement of evapotranspiration and soil moisture is more difficult and expensive. Soil moisture can be measured with gravimetry, lysimetry, radiological techniques such as neutron scattering, or dielectricity based reflectometry (WMO, 2008), whereas ET is usually indirect measured through water budget methods. The direct Pan-evaporation measurement givens only an approximation of free-water evaporation, which need to be adjusted empirically to obtain free-water evaporation under natural conditions. Eddy-correlation measurements are often considered to be the "true" ET rate, however it is not applicable for routine measurement because of its stringent instrumentation requirements. The strong spatial variation of ET and soil moisture with the local meteorological and hydrological conditions, referred by Western et al. (2002) as scale effect, together with the high cost of measurements, render all types of point measurements impractical for an extensive spatial measurements.

Methods based on remote sensing are nowadays widely deployed to measure soil moisture and to derive evapotranspiration. Three types of microwave sensors with different wavelength are used to capture soil moisture information from space: radiometers, Synthetic Aperture Radars (SARs), and scatterometers. Wagner et al. (2007) conclude that the operational coarse-resolution (25~50 km) soil moisture products can be expected within next few years from radiometer and scatterometer systems, yet operational soil moisture retrieval at finer scale (≤ 1 km) from SAR still need technological breakthroughs. The main limitations for the operational soil moisture remote sensing are the interfering signal of soil surface roughness and vegetation canopy, and the restricting signal penetration depth (Western et al., 2002). An alternative of inferring

HESSD
8, 7055–7090, 2011

evapotranspiration with modeling approach using other remotely sensed parameters, such as land surface temperature (LST), vegetation index (NDVI/EVI), etc. are widely used (Cleugh et al., 2007; Wang et al., 2007; Mu et al., 2007).

Many methods exist for PET evaluation. Empirical equations based on simple meteorological input are widely used to estimate regional ET. Xu and Singh (2000) provided an overview of the temperature and radiation based method. Other empirical methods utilize the remotely sensed LST and vegetation index data to calculate the the actual evapotranspiration, such as triangle method (Price, 1990), B-method (Carlson et al., 1995), temperature/vegetation dryness index (TVDI) (Andersen et al., 2002). A good overview of the remote sensing based techniques can be found in Verstraeten et al. (2008). More physical approaches are based on the conservation of either energy, mass or both. Penman-Monteith method, also called combination method, because it eliminates the surface temperature and does not need an explicit calculation of sensible heat flux, is the most popular approach used in modeling the physical process of ET. The surface energy balance method, usually applied in land surface models (LSM), on the contrary, tries to employ remotely sensed LST data to derive aerodynamic surface temperature and to explicitly determine sensible heat flux, so that the latent heat flux associated with ET can be calculated as a residual (Bastiaanssen et al., 1998; Su, 2002).

This paper applies the Soil Water Atmosphere Plant (SWAP) model to investigate the spatial ET/SMC variability originates from spatial wind and radiation difference. First a brief introduction of the SWAP model will be given. Because the SWAP model utilizes a Penman-Monteith approach for ET estimation, a short review of sensitivity analysis of PM equation is summarized prior to the model application, aiming to give some justification of the study of wind and radiation. Then the possibility of the application of MODIS LAI data with the model is examined. Finally the numerical experiments with the SWAP model is performed. To test solely the spatial radiation effect, all other parameters at each grid are holding the station observed values except radiation. So does for the wind. The ET/SMC resulting from the interaction of spatial wind and radiation are also examined with both parameters assuming spatial variant input. The experiments with land-use specific LAI are tested to approximate the topographic induced ET variability under more realistic conditions. The impact of soil type on ET has been also investigated with point experiments.

2 Study area and data

The study is focusing on the topographic effects on ET/SMC, i.e. the water exchange and transfer in vertical direction assuming no horizontal/lateral flow. A delineated water basin is not necessary in this case. Instead, a region with rich topographic features, e.g. an area with complex terrain is required to reflect a wide topographic effect. A rectangular region contains both mountains and flood plains in Southern Germany is taken as the study area for our purpose (see Fig. 1). For this larger area, simulations are done at 1000 m resolution. A small area on the north-east mountain part of the study area is taken for detailed study, and simulation are performed at 100 m resolution.

The original land use of the study area are defined by 16 classes. For wind simulation, the land use is re-classified into 9 groups as specified in the METRAS PC model (Schlünzen et al., 2001). To further simplify the parameterization of evapotranspiration modeling, similar land use are again merged into one class assigned with unique parameter sets in the SWAP model. The final land use map consists of 5 land use types – grass, agriculture, deciduous forest, coniferous forest, and others, which stands for residence and industrial area in the original land use map. In this study such area are assigned with parameters of bare soil.

2.1 Meteorological data

Daily spatial radiation and wind patterns of year 2002 are obtained using *r.sun* model (Hofierka and Suri, 2002) and METRAS PC model respectively, both with globally available data. The wind field is simulated under the consideration of surface roughness

HESSD
8, 7055–7090, 2011
Topographic effects on spatial ET and soil moisture
M. Liu et al.

caused by land use difference. Figure 2 shows the daily spatial variation expressed by $\frac{P_{90}-P_{10}}{\mu_s}$ over the year . The wind fields of both inner and outer domain are simulated at 1000m resolution. For both area, the difference between the lower and upper 10 quartile of wind force can be as high as two times the mean wind force for some days. For radiation, the inner domain is simulated with 100m resolution, whereas the outer domain is simulated at 1000m resolution. In addition to the variance of actual radiation, the variance of potential radiation is also displayed in the figure by the solid line. Except in very few winter days, the spatial variation of potential radiation is normally larger than the variation of actual radiation. Because of the finer resolution of the inner domain, the relative radiation difference is up to 90 %, whereas the outer domain shows a maximum relative difference of 15 %. To avoid the reduced spatial radiation variability resulted from a coarse DEM resolution, the aggregated actual radiation from 500m and 100m resolution is applied, and plotted for the sake of comparison. It shows that except in the summer time, the spatial variance of aggregated radiation from 500m simulation is almost doubled of the direct 1000m simulation, whereas the improvement with aggregation from 100m simulation to 1000m is marginal. Therefore, in this work the aggregated radiation from simulation with 500m resolution will be used. The spatial variation of both solar and wind are more stable in summer season, and vary strongly in winter season.

Table 1 shows the spatial variation of the mean daily radiation, both potential and actual, and wind of both domains. The mean potential radiation shows a much higher variation then the mean actual radiation. For radiation, because of the finer resolution of the inner domain, the spatial variation of inner domain is much larger than the outer domain. But for wind, under the same resolution, the outer domain shows higher variation, because the outer domain contains more diversified topographic features.

To investigate the spatial ET/SMC variability caused by wind and radiation, all other inputs are assuming spatially homogeneous values, which means one station observation for these inputs is enough. Temperature and precipitation data are obtained from the station Rottenburg-Kiebingen for the year 2002. Because the station does

HESSD
8, 7055–7090, 2011

not provide humidity, these data are taken from the nearest meteorological station Stuttgart-Echterdingen. In case humidity data is not available, it can also be estimated with temperature data (Thornton et al., 1997). First dew-point temperature T_d [°C] is approximated by minimum daily temperature T_{min}. Then the ambient vapor pressure e_a can be derived from T_{min}, and the saturated vapor pressure e_s can be evaluated at the mean daily temperature T_a, which can be expressed as a weighted average of max daily temperature T_{max} and minimum daily temperature T_{min} (see Eqs. 1–3).

$$e_a = 0.611 \exp\left(\frac{17.3\,T_{min}}{237.3+T_{min}}\right) \quad (1)$$

$$e_s = 0.611 \exp\left(\frac{17.3\,T_a}{237.3+T_a}\right) \quad (2)$$

$$T_a = 0.606\,T_{max} + 0.394\,T_{min} \quad (3)$$

2.2 Land use data and LAI

Leave Area Index (LAI) required by the SWAP model are obtained from MODIS 8-day composite data (Yang et al., 2006). A preliminary investigation of the MODIS LAI data shows, the cell-based LAI values show a strong fluctuation, which may come from the data uncertainty. Figure 3 shows LAI of two randomly selected points. To remove the strong time variation, the land use specific LAI, which is the spatial average value of the same land use, is applied. As shown in Fig. 1, the study area are dominated by several land use types, the 16 land use types are aggregated into 5 main land use types: grass, agriculture, coniferous forest, deciduous forest, and others. The right figure in Fig. 3 shows the land use specific LAI, and the time varying feature is reduced.

3 The SWAP model

The SWAP model is an agro-hydrological model that simulates transport of water, solutes and heat in saturated/unsaturated soils (van Dam et al., 1997). SWAP is designed ideally for field scale study, but it can also be applied to regional scale. It considers a

HESSD
8, 7055–7090, 2011

one-dimensional column in the vertical direction, with the lower atmospheric layer being the upper boundary and the unsaturated zone or the upper part of the saturated zone being the bottom boundary. The soil water flow is simulated by the Richard's Equation discretized in a finite difference scheme. Three potential rates are modeled by the Penman-Monteith algorithm by varying the crop resistance, crop height and albedo: potential ET of wet crop (ETP_w), potential ET of dry crop (ETP_d), and potential evaporation of bare soil (EP_s), based on which the actual rates of a fully covered or non-covered surface can be calculated. For partly covered soils, the potential ET of wet or dry crop is partitioned into potential evaporation (EP) and potential transpiration (TP) according to soil cover fraction (SC) as shown in Eq. (4) or the energy interception by LAI of the vegetated area (see Eq. 5) .

$$\mathrm{EP} = (1 - \mathrm{SC})\mathrm{EP_s} \tag{4}$$

$$\mathrm{EP} = \mathrm{EP_s} e^{-\kappa_{\mathrm{gr}}\,\mathrm{LAI}} \tag{5}$$

$$\mathrm{TP} = \mathrm{ETP_d} - \mathrm{EP} \tag{6}$$

Here, κ_{gr} is the extinction coefficient for solar radiation. The actual transpiration is the integrated root water uptake of each root layer taking into the reduction due to water and/or salinity stress. In absence of any stress, the total root uptake capacity equals to the potential transpiration rate.

$$\mathrm{RX_p}(z) = \frac{l_{\mathrm{root}}(z)}{\int_{-D_{\mathrm{root}}}^{0} l_{\mathrm{root}}(z)\mathrm{d}z}\mathrm{TP} \tag{7}$$

$$\mathrm{RX_a}(z) = \alpha_{\mathrm{r}}\,\mathrm{RX_p}(z) \tag{8}$$

$$\mathrm{TA} = \int_{-D_{\mathrm{root}}}^{0} \mathrm{RX_a}(z)\mathrm{d}z \tag{9}$$

where $l_{\mathrm{root}}(z)$ and $\mathrm{RX_p}(z)$ is root density and the potential root water extraction rate at depth z. *D*root is the root layer thickness, α_{r} is the reduction factors due to water, salinity stress and frozen conditions. $\mathrm{RX_a}(z)$ and TA is the differential and integrated actual transpiration respectively.

HESSD
8, 7055–7090, 2011

Figure 4 shows the example of water stress coefficient α_{rw} as a function of soil water pressure head. The water stress caused reduction of transpiration is depicted in Fig. 4. In the range $h_3 < h < h_2$ root water uptake is optimal. Below h_3 root water uptake linearly declines until zero at h_4 (permanent wilting point). The threshold pressure h_3 increases with potential transpiration rates. For low potential transpiration $\mathrm{TP}_{\mathrm{low}}$, the threshold pressure h_{3l} is lower than the threshold pressure h_{3h} at high potential transpiration rate TP_{high}. Above h_2 root water uptake linearly decreases due to insufficient aeration until zero at h_1. In this study, the recommended values from SWAP manual is taken, which usually allows a wide range of optimal uptake. The crop specific parameters are listed in Table 2.

The maximum soil evaporation $E_{\max}$ is restricted by the soil water suction at the top soil layers based on Darcy's law:

$$E_{\max} = K_{1/2}(\theta)\left(\frac{h_{\mathrm{atm}} - h_1 - z_1}{z_1}\right) \tag{10}$$

where $K_{1/2}(\theta)$ [$\mathrm{cm} \times \mathrm{d}^{-1}$] is the average hydraulic conductivity between the soil surface and the first node as a function of soil water saturation θ [-], h_{atm} is the soil water pressure head [cm] in equilibrium with the air relative humidity, h_1 is the soil water pressure head of the first node, and z_1 is the soil depth [cm] at the first node. SWAP provides also the option to choose empirical evaporation functions of Black et al. (1969) and Boesten and Stroosnijder (1986). In the SWAP model, the actual soil evaporation EA is determined by the minimum value of EP, $E_{\max}$, or results of the empirical functions. The soil water head and hydraulic conductivity under unsaturated condition are modeled following the Mualem-van Genuchten functions as following.

$$S_\mathrm{e} = (1 + |\alpha_\mathrm{vg} h_\mathrm{suc}|^{n_\mathrm{vg}})^{-m_\mathrm{vg}} \tag{11}$$

$$m_\mathrm{vg} = 1 - \frac{1}{n_\mathrm{vg}} \tag{12}$$

$$K_\mathrm{e} = K_\mathrm{sat} S_\mathrm{e}^{\lambda_\mathrm{vg}} (1 - (1 - S_\mathrm{e}^{1/m_\mathrm{vg}})^{m_\mathrm{vg}})^2 \tag{13}$$

$$S_\mathrm{e} = \frac{\theta_\mathrm{e} - \theta_\mathrm{res}}{\theta_\mathrm{sat} - \theta_\mathrm{res}} \tag{14}$$

with	S_e	:	effective saturation [–]
	h_suc	:	soil water head [L]
	α_vg	:	parameter related to the modal pore size –]
	n_vg	:	parameter of pore-size distribution [–]
	m_vg	:	parameter of pore-size distribution [–]
	K_e	:	effective hydraulic conductivity [$\mathrm{L\,T^{-1}}$]
	K_sat	:	saturated hydraulic conductivity [$\mathrm{L\,T^{-1}}$]
	λ_vg	:	shape parameter [–]
	θ_e	:	effective volumetric water content [$\mathrm{L^3\,L^{-3}}$]
	θ_res	:	residual volumetric water content [$\mathrm{L^3\,L^{-3}}$]
	θ_sat	:	saturated volumetric water content [$\mathrm{L^3\,L^{-3}}$]

Soil in the study region are mainly clay (soil A) and loam (soil B), their hydraulic parameters are shown in Table 3. Besides the actual soil conditions, the study also investigates the effects of soil types on ET/SMC by simulating with a more permeable soil configuration (soil C and soil D in Table 3).

HESSD
8, 7055–7090, 2011

4 Sensitivity analysis of Penman-Monteith equation

Sensitivity analysis can estimate the relative response of each input factors. Frey and Patil (2002) and Saltelli et al. (2006) provide a good overview of approaches available for sensitivity test. Sensitivity analysis of Penman-Monteith actual ET have been investigated for three sites in UK by Beven (1979) with the nominal range sensitivity analysis, i.e. by individually varying only one of the model input while holding all other inputs at their nominal or base-case values (Cullen and H.C., 1999). Recently Bois et al. (2008) applied the more advanced Sobol's method, which enables the evaluation of the interaction between the input variables. The Sobol's method decompose the total variance V of the model output into variance with different orders in response to individual or simultaneous variation of the model inputs. For a model with k input variables, $2^k - 1$ variance terms can be obtained:

$$V = \sum_i V_i + \sum_{i<j} V_{ij} + \sum_{i<j<m} V_{ijm} + \cdots + V_{1,2,\ldots,k} \tag{15}$$

where V_i is the first-order variance in response to variation of the ith input variable, and V_{ij} is the second-order variance to the simultaneous change of the ith and the jth model input, and so-on. The Sobol's sensitivity index, which measures the model output variance caused the ith model input, including all the possible interactions with other inputs, is defined as:

$$S_{T_i} = \frac{V_i + \sum_j V_{ij} + \sum_{j<m} V_{ijm} + \cdots + V_{i,j,\ldots,k}}{V} \tag{16}$$

Bois et al. (2008) have shown that wind speed has a major impact on ET during winter season and solar radiation is more influential during summer, whereas other meteorological parameters show no significant effects. The analysis is achieved with the SIMLAB software (Saltelli et al., 2007), which will not be repeated here.

HESSD
8, 7055–7090, 2011

5 Numerical experiments and results

5.1 Model setup

To simulate the actual ET with SWAP, not only the meteorological input, but also detailed the soil hydraulic information, vegetation leaf and root properties, and groundwater dynamics are required. The soil hydraulic parameters and the vegetation properties are extremely heterogeneous, and are associated with high uncertainty. Spatial acquisition of such data are very expensive, if not impossible. The aim of this work is to seek the theoretical pattern caused by decisive topographic-induced spatial patterns of radiation and wind, therefore a resort of spatial soil-vegetation data is not necessary. Nevertheless, the application of the actual spatial data will lead to a better approximation of the actual spatial ET/SMC patterns, therefore a maximum utilization of the actual data is attempted in this work with the application of remote sensing data. The numerical experiments are conducted at two different resolutions, $100 \times 100\,\mathrm{m}^2$ for the inner domain and $1 \times 1\,\mathrm{km}^2$ for the outer domain to check the scale effect. For all simulations and each grid, the boundary and initial conditions are set to be identical, and are set as following:

- Bottom boundary condition: a shallow groundwater aquifer of 3m on top of an impervious layer is assumed for the region, thus each grid, which implies a zero bottom flux boundary. A simplification of regional groundwater table is assumed – groundwater depth is linearly related to the local elevation, with a groundwater depth of 0.7m at the lowest elevation close to the river, and a depth of 1.5m at the highest elevation;
- Lateral drainage condition: groundwater dynamics caused by groundwater flow is considered to be equivalent to drainage to surface water with drainage bottom at 5cm below the groundwater table;

HESSD
8, 7055–7090, 2011

- Soil hydraulic properties: the upper 2m soil consisting of an upper 30cm less permeable clay and an underlying 170cm more permeable loam (see Table 3), is considered in the simulation.

Meteorological data, such as temperature, precipitation, and humidity are station observations at Rottenburg-Kiebingen. Station radiation and wind data from Stuttgart station is used in case that spatially constant value is required for a given experiment. Both fictitious homogeneous vegetation data and actual remote sensing LAI have been used depending on the experiment objective. Following numerical experiments have been tested:

- Experiment 1: spatial actual radiation, station wind, homogeneous vegetation of grass;
- Experiment 2: station radiation, spatial wind, homogeneous vegetation of grass;
- Experiment 3: spatial actual radiation, spatial wind, homogeneous vegetation of grass;
- Experiment 4: spatial actual radiation, spatial wind, actual land use;

5.2 Simulation results

5.2.1 Point results

Two points, P1 and P2 (see Fig. 1a), with distinct topographic features are chosen for comparison. P1 is located at the north side of the mountain foot, whereas P2 is located in south aspect of the mountain peek. The topographic information of the two points are listed in Table 4. Figure 5 shows the common (see Fig. 5a) and specific meteorological inputs obtained at 100m scale (see Fig. 5b) at the two selected points. P2 receives considerably higher radiation and exposed to stronger wind (see Fig. 5b). Both points are simulated by assuming a vegetation cover of natural grass. Figures 5c

HESSD
8, 7055–7090, 2011

and 5d show that the soil moisture dynamics of the two points simulated at the spatial resolution of 100m. The soil moisture profile of the both points are similar, but point P2 is much drier than point P1. The driest period is from 24 March to 11 April, during which there is no rainfall in around two weeks.

Table 4 shows the water balance at the two points simulated with two different soil configurations, a less permeable soil conditions (soil A & B) and a highly permeable soil conditions (soil C & D). The simulation is done for two different scales, 100m and 1000m. At both scale, more water are evaporated/transpired at P2 than P1. At P1 more water is drained through groundwater and/or surface runoff than at P2. The highly permeable soil allows strong infiltration, therefore most water are drained through subsurface, and very little surface runoff is generated. There is no big difference between the actual and the potential evapotranspiration, because southern Germany is a humid region, where ET is a energy limited process other than a water availability limited process. The actual transpiration is more close to the potential value, and in the case of more permeable soil conditions, they are even identical, which is resulted from the strong water transportation capacity of plants than soil texture. As shown in the table, simulation at coarser resolution diminishes the difference between the two locations. At 100m resolution, the difference of potential and actual ET at the two points are around 23.7 % and 20.6 % respectively, while at 1000m resolution the difference are around 14.9 % and 13.7 % respectively. The soil condition does not change the total actual ET much, but the partition between evporation and transpiration. In the case of highly permeable soil, the soil transportation capacity is much weaker than the less permeable clay and loam, therefore the soil evporation is reduced, and the available energy is consumed by plants and increases the amount of tranpiration.

5.2.2 Spatial results

The spatial variabilities at different scales are also investigated. Figures 6a and 6b show the spatial variability of the spatial radiation and wind by the probability density function (PDF). Figures 6c, 6d and 6e show the PDFs of the yearly total evaporation,

HESSD
8, 7055–7090, 2011

transpiration, and evapotranspiration of the respective numerical experiments. The results of Experiment 4 spread much wider than the others because of the variation of vegetation types, they are shown individually in Fig. 6f to avoid the distortion of other experiment results in the figure. To be mentioned, the negative value in Fig. 6f is an artifacts coming from the kernel smoothing of the distribution curve, when zero transpiration of bare soil occurs in the data.

Figure 7 shows the spatial variation of radiation (Fig. 7a), wind (Fig.7b), EA (Fig. 7c), TA (Fig.7d), ETA (Fig. 7e) and the results with actual land use (Fig. 7f) for the inner domain at finer scale. The PDF of Experiment 1 which considers only radiation effects, both evaporation and transpiration spread much narrower than the PDF of other experiments. For both domains, especially for the outer domain, the result of Experiment 2 is very close to Experiment 3, which reflects the domination of the wind effects over the radiation effects. The variation caused by different vegetation can also be observed through the multiple peeks in the PDFs in Figs. 6f and 7f. Because in general, agriculture field has the highest ET and ET is decreasing in the order of grass, deciduous forest, pine forest, and bare soil. Experiment 4 with actual land use gives less ET than Experiment 3 with natural grass only. Not only the amount of total ET, the partition between evaporation and transpiration also changes with plant type, e.g. forest shows higher transpiration because of the strong root uptake capability and higher vegetation cover of soil.

The spatial variation quantified by $\frac{P_{90}-P_{10}}{\mu_s}$ is shown in Tables 5 and 6. The variation of ET is much smaller than the variation of energy input, i.e. wind and solar radiation, because of the nonlinearity of the process. The inner domain has a larger variation in radiation and a smaller variation in wind, therefore the resulted variation by radiation of the inner domain is much larger than the outer domain, and *vice versa*, the variation originated from wind is smaller. The inner domain shows also a higher yearly area mean ET than the outer domain, because it is lying on a mountainous region.

Figuers 8a, b, c, d show the resulted spatial actual ET of the four numerical experiments respectively. The data in the inner catchment are shown in the color scale of the

HESSD
8, 7055–7090, 2011

outer domain. The strong contrast within the inner domain shows that the fine scale simulation captures the spatial variation better. The extreme low ET represented by the lower tail in the PDFs in Figs. 6 and 7 occurs exclusively the on the north side of steep mountains and in river valleys, where sunshine is shielded. Such small area may not be very significant for rainfall-runoff generation process, but is ecologically very important. Under homogeneous land use, the patterns of ET demonstrate a strong structured feature which is related to the topography. When land use is considered, the heterogeneity of ET is strongly related to land use type (see Fig. 8d). Figure 8e shows the soil moisture of upper 20cm on 8 April, which is the end of around two weeks dry weather in the spring. The soil moisture is strongly related to the topography, which comes from the assumption of elevation related groundwater table.

Figure 9 shows the monthly actual areal ET (see Fig. 9a) and the spatial variation of actual ET over the year (see Fig. 9b) for the outer domain resulted from Experiment 3 when both spatial wind and radiation are considered. In the winter time, although the amount of evapotranspiration is relatively small, the variation in terms of $\frac{P_{90}-P_{10}}{\mu_s}$ is as high as 180 %, which may also imply a strong effect on snowmelt.

6 Discussion

In this paper, numerical experiments have been applied to a mountainous region at two different scales to simulate ET and SMC as a more advanced sensitivity test of the factors involved in ET processes, as theoretical sensitivity analysis of the Penman-Monteith equation shows that both solar radiation and wind are important factors in the ET processes. The study aims at analyzing the spatial variability of ET/SMC caused by spatial radiation, wind, and their interaction. Simulations with spatial vegetation information obtained from MODIS LAI are also performed to check the effect of spatial vegetation distribution on ET/SMC. The result shows that, under the humid climate condition of the study area, ET is an energy controlled process. A spatial ET pattern exists, and in the case of homogeneous land use, it is well related to topography. When heterogeneous land uses present, ET pattern is strongly controlled by land use type. Different soil conditions will change the partition between evaporation and transpiration and, partition between surface runoff and subsurface flow, but has very limited impact on total amount of ET and runoff. Radiation causes a stronger spatial variation of ET/SMC at finer scale than at coarser scale, especially for evaporation. But under homogeneous land use, spatial wind effect is dominating the spatial radiation difference at both scales. Because of the nonlinearity of the evapotranspiration process, the resulted spatial variation is smaller than the variation in the meteorological inputs. The spatial variation is much stronger in the winter time, which may cause a very different snowmelt progress. The spatial difference in ET is offset by the amount of runoff generated, which may have an implication in flood generation.

The SWAP model is applied with radiation and wind data mapped from global data and physically-based model, which demand very few observation data. Because the lack of groundwater data, a linear groundwater table is assumed for the numerical experiments in this study. In order to implement a complete spatial simulation, the SWAP model should be coupled with a groundwater model, to update the groundwater level at each time step.

This study has confirmed the effects of topographic induced spatial radiation and wind on ET, and this information may be utilized to improve hydrological concepts in ET/SMC modeling. Moore et al. (1993) derived a dimensionless evaporation scaling ratio based on spatial radiation differences. Vertessy et al. (1990) developed a radiation weighted wetness index, which is a combination of potential solar radiation index (the ratio of the potential solar radiation on a sloping surface to that on a horizontal surface) and wetness index. As we have seen, that the wind effect is much stronger than radiation, so the author call for the inclusion of wind effect into the wetness index following a similar approach to Vertessy et al. (1990).

Acknowledgements. The authors would like to acknowledge the International Postgraduate Studies in Water Technologies (IPSWaT) scholarship funded by German Federal Ministry of Education and Research (BMBF) for the support of this PhD research.

HESSD
8, 7055–7090, 2011

References

Andersen, J., Sandholt, I., Jensen, K. H., Refsgaard, J. C., and Gupta, H.: Perspectives in using a remotely sensed dryness index in distributed hydrological models at the river-basin scale, Hydrol. Process., 2987, 2973–2987, doi:10.1002/hyp.1080, 2002. 7059

Bastiaanssen, W. G. M., Menenti, M., Feddes, R. A., and Holtslag, A. A. M.: A remote sensing surface energy balance algorithm for land (SEBAL). 1. Formulation, J. Hydrol., 212–213, 198–212, doi:10.1016/S0022-1694(98)00253-4, 1998. 7059

Beven, K.: A sensitivity analysis of the Penman-Monteith actual evapotranspiration estimates, J. Hydrol., 44, 169–190, doi:10.1016/0022-1694(79)90130-6, 1979. 7066

Black, T. A., Gardner, W. R., and Thurtell, G. W.: The prediction of evaporation, drainage and soil water storage for a bare soil, Soil Sci. Soc. Am., 33, 655–660, 1969. 7064

Boesten, J. and Stroosnijder, L.: Simple model for daily evaporation from fallow tilled soil under spring conditions in a temperate climate, Neth. J. Agr. Sci., 34, 75–90, 1986. 7064

Bois, B., Pieri, P., Leeuwen, C. V., Wald, L., Huard, F., Gaudillere, J.-P., and Saur, E.: Using remotely sensed solar radiation data for reference evapotranspiration estimation at a daily time step, Agr. Forest Meteorol., 148, 619–630, doi:10.1016/j.agrformet.2007.11.005, 2008. 7066

Bresnahan, P. A. and Miller, D. R.: Choice of data scale: predicting resolution error in a regional evapotranspiration model, Agr. Forest Meteorol., 84, 97–113, 1997. 7057

Carlson, T. N., Capehart, W. J., and Gillies, R. R.: A new look at the simplified method for remote sensing of daily evapotranspiration, Remote Sens. Environ., 54, 161–167, doi:10.1016/0034-4257(95)00139-R, 1995. 7059

Cassardo, C., Balsamo, G. P., Cacciamani, C., Cesari, D., Paccagnella, T., and Pelosini, R.: Impact of soil surface moisture initialization on rainfall in a limited area model: a case study of the 1995 South Ticino flash flood, Hydrol. Process., 16, 1301–1317, 2002. 7057

Cleugh, H. A., Leuning, R., Mu, Q., and Running, S. W.: Regional evaporation estimates from flux tower and MODIS satellite data, Remote Sens. Environ., 106, 285–304, 2007. 7059

Cullen, A. and H.C., F.: Probabilistic techniques in exposure assessment, Plenum Press, 1999. 7066

Dingman, S. L.: Physical Hydrology, Prentice-Hall, Inc., 2 Edn., 2002. 7056

FAO: Expert consultation on revision of FAO methodologies for crop water requirements, ANNEX V: FAO Penman-Monteith Formula, Tech. rep., FAO, Rome, Italy, 1990. 7057

HESSD

8, 7055–7090, 2011

Topographic effects on spatial ET and soil moisture

M. Liu et al.

Frey, H. C. and Patil, S. R.: Identification and review of sensitivity analysis methods, Risk Analysis, 22, 553–578, doi:10.1111/0272-4332.00039, 2002. 7066
Hofierka, J. and Suri, M.: The solar radiation model for Open source GIS: implementation and application, in: Proceddings of the Open source GIS – GRASS users conference 2002, Trento, Italy, 2002. 7060
Moore, I. D., Gallant, J. C., and Guerra, L.: Modelling the spatial variability of hydrological process using GIS, in: HydroGIS 93: Application of Geographic Information System in Hydrology and Water Resources, Proceedings of Viena Conference, IAHS Publication, 1993. 7072
Mu, Q., Heinsch, F. A., Zhao, M., and Running, S. W.: Development of a global evapotranspiration algorithm based on MODIS and global meteorology data, Remote Sens. Environ., 111, 519–536, doi:10.1016/j.rse.2007.04.015, 2007. 7059
Norbiato, D., Borga, M., Esposti, S. D., Gaume, E., and Anquetin, S.: Flash flood warning based on rainfall thresholds and soil moisture conditions: An assessment for gauged and ungauged basins, J. Hydrol., 362, 274–290, 2008. 7057
Penman, H. L.: Natural evaporation from open water, bare soil and grass, Proc. Roy. Soc., A193, 120–146, 1948. 7057
Price, J.: Using Spatial Context in Satellite Data to Infer Regional Scale Evapotranspiration, IEEE T. Geosci. Remote, 28, 940–948, 1990. 7059
Saltelli, A., Ratto, M., Tarantola, S., and Campolongo, F.: Sensitivity analysis practices: Strategies for model-based inference, Reliab. Eng. Syst. Safe., 91, 1109–1125, doi:10.1016/j.ress.2005.11.014, 2006. 7066
Saltelli, A., Tarantola, S., Campolongo, F., and Ratto, M.: Sensitivity analysis in practices: A guide to assessing scientific models, Wiley, 2007. 7066
Schlünzen, K. H., Bigalke, K., Lüpkes, C., and Panskus, H.: Documentation of the mesoscale transport- and fluid model METRAS PC as part of model system METRAS+, Tech. rep., Meteorologisches Institut, Universitt Hamburg, mETRAS Technical Rep. 11, 2001. 7060
Su, Z.: The Surface Energy Balance System (SEBS) for estimation of turbulent heat fluxes, Hydrol. Earth Syst. Sci., 6, 85–100, doi:10.5194/hess-6-85-2002, 2002. 7059
Thornthwaite, C. W. and Mather, J. R.: The Water Balance, Publications in Climatology, 8, 188, 1955. 7056
Thornton, P. E., Running, S. W., and White, M. A.: Generating surfaces of daily meteorological variables over large regions of complex terrain, J. Hydrol., 190, 214–251, doi:10.1016/S0022-

1694(96)03128-9, 1997. 7062
van Dam, J., Huygen, J., Wesseling, J., R. A., F., Kabat, P., van Walsum, P., Groenendijk, P., and van Diepen, C.: Theory of SWAP version 2.0, Tech. rep., Department of Water Resources, Wageningen Agricultural University, Wageningen, the Netherlands, 1997. 7062
Verstraeten, W. W., Veroustraete, F., and Feyen, J.: Assessment of Evapotranspiration and Soil Moisture Content Across Different Scales of Observation, Sensors, 8, 70–117, 2008. 7059
Vertessy, R., Wilson, C., Silburn, D., Connolly, R., and Ciesiolka, C.: Predicting erosion hazard areas using digital terrain analysis, AHS AISH Publication, 192, 298–308, 1990. 7072
Wagner, W., Blöschl, G., Pampaloni, P., Calvet, J.-C., Bizzarri, B., Wigneron, J.-P., and Kerr, Y.: Operational readiness of microwave remote sensing of soil moisture for hydrologic applications, Nord. Hydrol., 38, 1–20, 2007. 7058
Wang, K., Wang, P., Li, Z., Cribb, M., and Sparrow, M.: A simple method to estimate actual evapotranspiration from a combination of net radiation , vegetation index , and temperature, J. Geophys. Res., 112, 1–14, doi:10.1029/2006JD008351, 2007. 7059
Western, A. W., Grayson, R. B., and Blöschl, G.: Scaling of Soil Moisture: A Hydrologic Perspective, Annu. Rev. Earth Pl. Sci., 30, 149–180, 2002. 7057, 7058
WMO: Guide to Meteorological Instruments and Methods of Observation, World Meteorological Organization, 7 Edn., 2008. 7058
Xu, C. Y. and Singh, V. P.: Evaluation and generalization of radiation-based methods for calculating evaporation, Hydrol. Process., 14, 339–349, 2000. 7059
Yang, W., Tan, B., Huang, D., Rautiainen, M., Shabanov, N. V., Wang, Y., Privette, J. L., Huemmrich, K. F., Fensholt, R., Sandholt, I., Weiss, M., Ahl, D. E., Gower, S. T., Nemani, R. R., Knyazikhin, Y., and Myneni, R. B.: MODIS Leaf Area Index Products: From Validation to Algorithm Improvement, IEEE T. Geosci. Remote, 44, 1885–1898, 2006. 7062

HESSD
8, 7055–7090, 2011

Topographic effects on spatial ET and soil moisture

M. Liu et al.

Table 1. Spatial variability of mean daily wind and radiation.

	Potential radiation	Actual radiation	wind
Inner domain	21.16 %	12.98 %	37.01 %
Outer domain	6.51 %	3.96 %	50.93 %

HESSD
8, 7055–7090, 2011

Table 2. Crop specific parameters for SWAP modeling.

	D_{root} [cm]	characteristic suction heads [cm]				
		h_1	h_2	h_{3h}	h_{3l}	h_4
Natural grass	60	0.0	−1.0	−200.0	−800.0	−8000.0
Maize	5~100	−15.0	−30.0	−325.0	−600.0	−8000.0
Pine forest	70	−0.0	−1.0	−600.0	−600.0	−6000.0
Deciduous forest	100	−1.0	−2.0	−600.0	−600.0	−6000.0

HESSD
8, 7055–7090, 2011

Table 3. Soil parameters for SWAP modeling.

	θ_{res} [cm^3 cm^{-3}]	θ_{sat} [cm^3 cm^{-3}]	α_{vg} [–]	n_{vg} [–]	K_{sat} [cm d^{-1}]	λ_{vg} [–]
Soil A	0.01	0.42	0.0099	1.288	2.36	−2.244
Soil B	0.01	0.42	0.0191	1.152	13.79	−1.384
Soil C	0.01	0.43	0.0227	1.548	9.65	−0.983
Soil D	0.02	0.38	0.0214	2.075	15.56	0.039

HESSD
8, 7055–7090, 2011

Table 4. Comparison of point simulation results with clay and loam.

	P1		P2	
	100m	1000m	100m	1000m
elevation [m]	616	608	820	811
aspect [degree]	315.0	6.92	194.5	188.8
slope [degree]	26.98	5.74	5.97	1.46
mean radiation [$MJ\,m^{-2}$]	9.33	10.54	12.25	11.98
mean wind [$m\,s^{-1}$]	1.73		3.10	
Acutal soil (Soil A & B)				
Initial water storage [mm]	801.5	802.1	786.0	786.7
transpiration [mm]	339.1(343.1)	357.1(360.9)	417.1(419.6)	414.1(416.6)
evaporation [mm]	154.3(197.4)	161.9(214.7)	177.7(248.8)	176.1(244.9)
drainage [mm]	509.7	486.7	411.5	416.3
runoff [mm]	88.0	85.9	78.7	78.9
Final water storage[mm]	816.8	817.1	807.4	807.8
Test soil (Soil C & D)				
Initial water storage [mm]	654.2	656.1	601.2	603.6
transpiration [mm]	344.3(344.3)	361.9(361.9)	421.7(421.7)	418.7(416.6)
evaporation [mm]	146.6(196.2)	153.2(213.6)	167.3(246.7)	165.8(244.9)
drainage [mm]	600.9	577.5	495.8	500.0
runoff [mm]	0.8	0.2	0.3	0.0
Final water storage[mm]	668.2	669.8	622.6	624.6

Note: the values in the parentheses are potential values.

HESSD
8, 7055–7090, 2011

Table 5. Numerical experiment results of outer domain.

	Spatial variation $\frac{P_{90}-P_{10}}{\mu_s}$ (%)							Annual area mean (mm)			
	EA	EP	TA	TP	ETA	ETP	SM*	EA	EP	TA	TP
EX 1	1.02	2.09	1.34	1.10	1.20	1.47	6.53	172.0	236.0	398.1	401.3
EX 2	4.90	6.20	8.95	9.33	7.95	8.00	7.35	170.9	233.9	393.5	396.7
EX 3	5.01	6.77	9.04	9.43	7.34	8.05	8.18	171.6	235.7	395.0	398.3
EX 4	62.23	113.72	33.54	39.69	19.39	24.60	34.65	150.6	228.9	336.1	359.9

[∗] Maximum daily spatial soil moisture variation over the year.

HESSD
8, 7055–7090, 2011

Topographic effects on spatial ET and soil moisture

M. Liu et al.

Table 6. Numerical experiment results of the inner domain.

	Spatial variation $\frac{P_{90}-P_{10}}{\mu_s}$ (%)							Annual area mean (mm)			
	EA	EP	TA	TP	ETA	ETP	SM*	EA	EP	TA	TP
EX 1	3.57	7.00	3.42	3.53	3.53	4.74	5.45	173.1	237.4	402.8	405.8
EX 2	4.09	5.07	7.14	7.39	6.35	6.36	6.21	172.6	236.7	400.4	403.4
EX 3	6.10	9.30	8.68	9.08	8.12	8.80	6.45	172.9	237.3	400.7	403.7
EX 4	77.53	148.17	28.83	31.65	18.35	22.88	33.34	134.3	180.7	374.7	377.96

[∗] Maximum daily spatial soil moisture variation over the year.

HESSD
8, 7055–7090, 2011

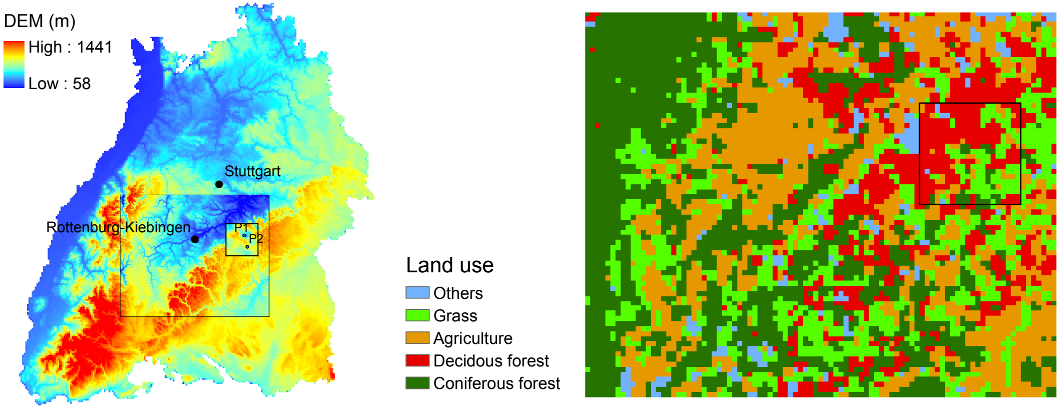

(a) Study area

(b) Land use in the study area

Fig. 1. Topography and land use of the study area.

HESSD
8, 7055–7090, 2011

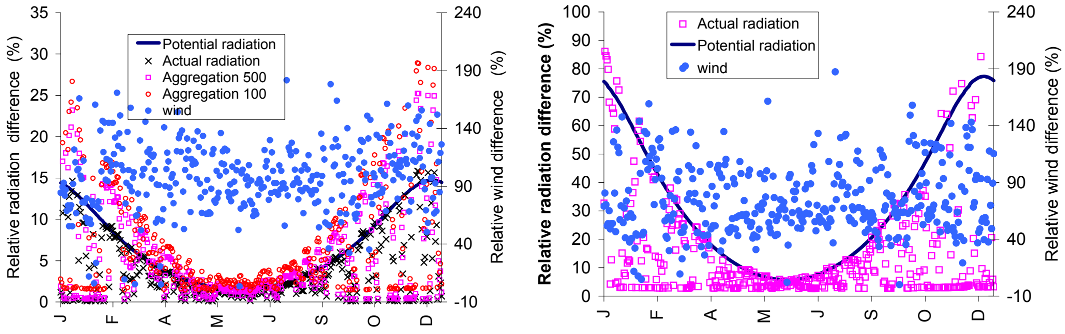

(a) Inner domain (b) Outer domain

Fig. 2. Spatial variation of wind and radiation over time.

HESSD
8, 7055–7090, 2011

Topographic effects on spatial ET and soil moisture

M. Liu et al.

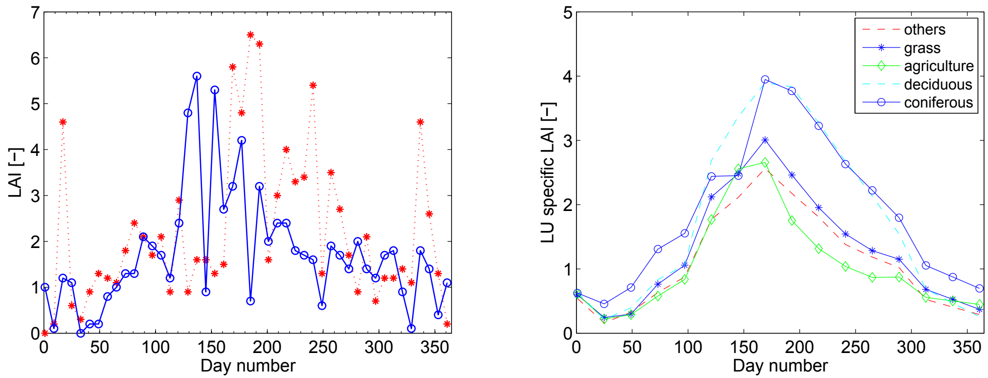

(a) LAI at two selected points

(b) Land use specific LAI

Fig. 3. Cell-based LAI (left) and land use specific LAI (right).

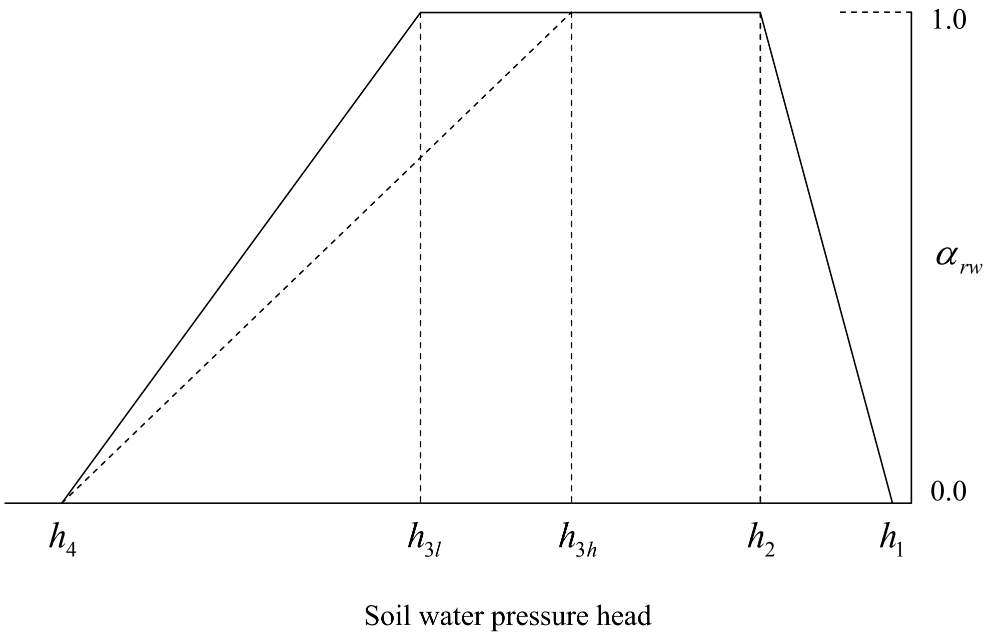

Fig. 4. Reduction coefficient for root water uptake.

HESSD
8, 7055–7090, 2011

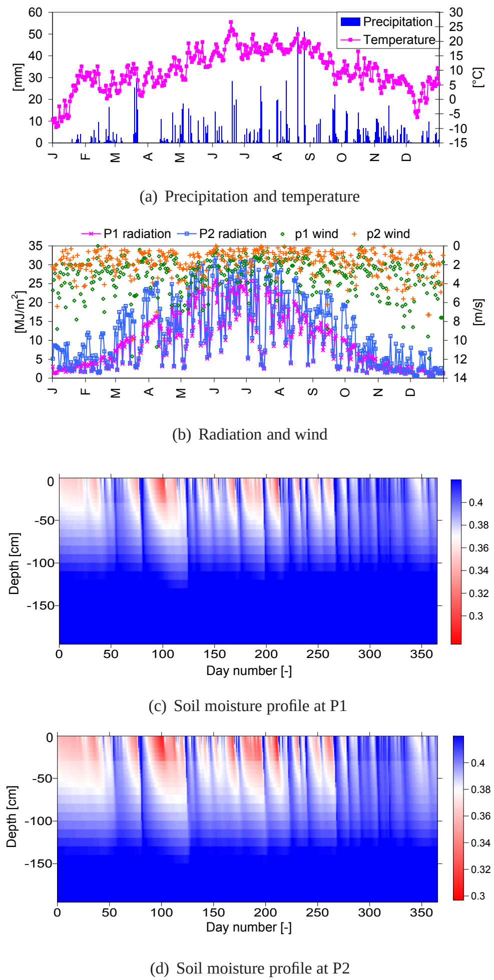

(a) Precipitation and temperature

(b) Radiation and wind

(c) Soil moisture profile at P1

(d) Soil moisture profile at P2

Fig. 5. Meteorological inputs and simulated soil moisture time series at P1 and P2.

HESSD

8, 7055–7090, 2011

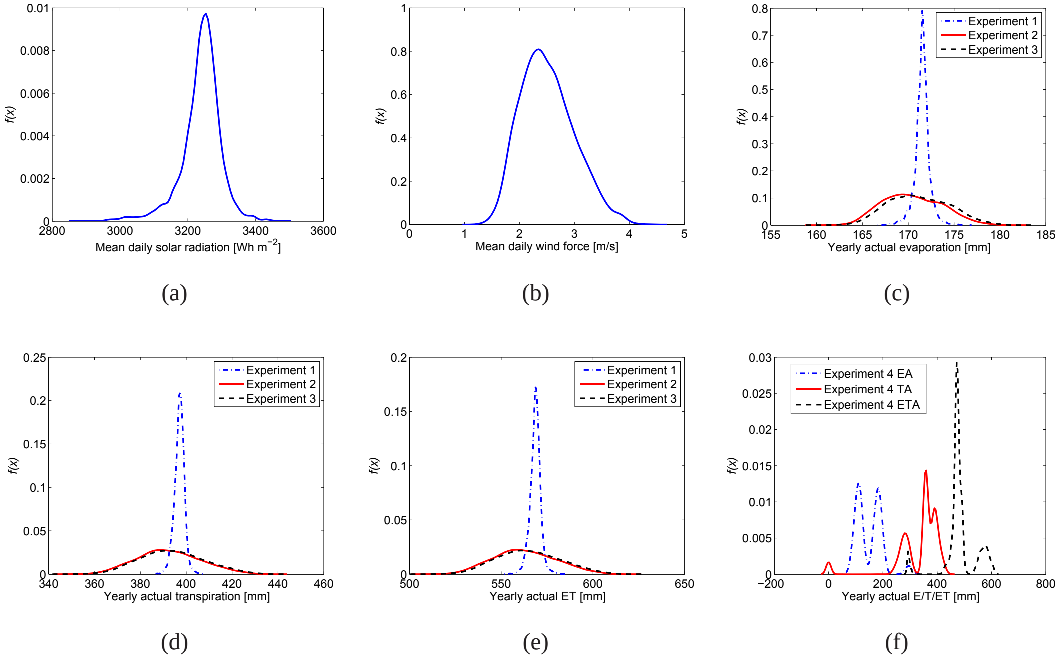

Fig. 6. Spatial variation of meteorological inputs and ET of outer domain.

HESSD
8, 7055–7090, 2011

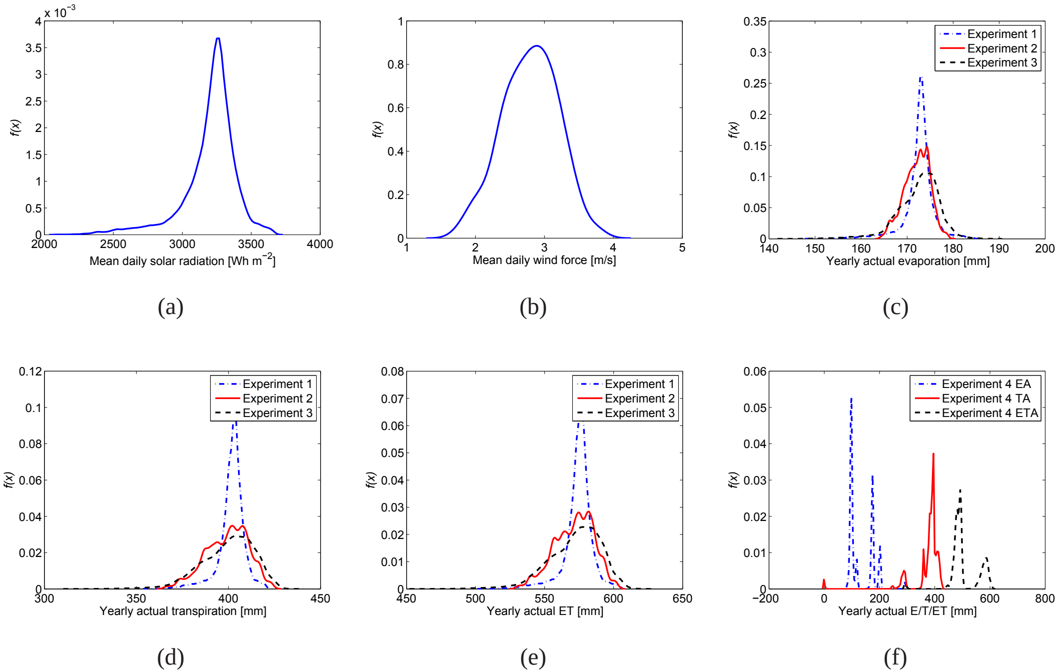

Fig. 7. Spatial variation of meteorological inputs and ET of inner domain.

HESSD

8, 7055–7090, 2011

Topographic effects on spatial ET and soil moisture

M. Liu et al.

Title Page
Abstract | Introduction
Conclusions | References
Tables | Figures
◄◄ | ►►
◄ | ►
Back | Close
Full Screen / Esc
Printer-friendly Version
Interactive Discussion

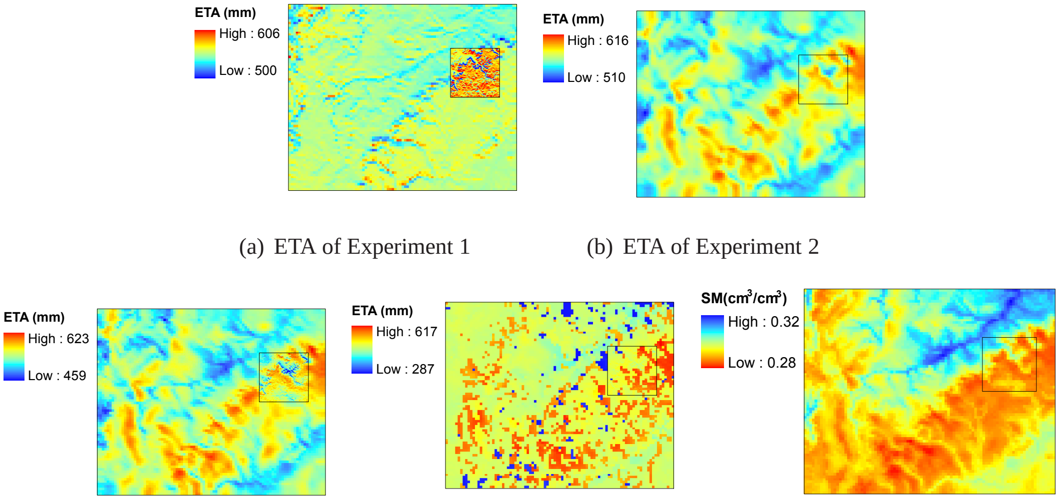

(a) ETA of Experiment 1

(b) ETA of Experiment 2

(c) ETA of Experiment 3

(d) ETA of Experiment 4

(e) SMC of Experiment 4 on day 101

Fig. 8. Spatial actual ET and SMC of the numerical experiments.

HESSD
8, 7055–7090, 2011

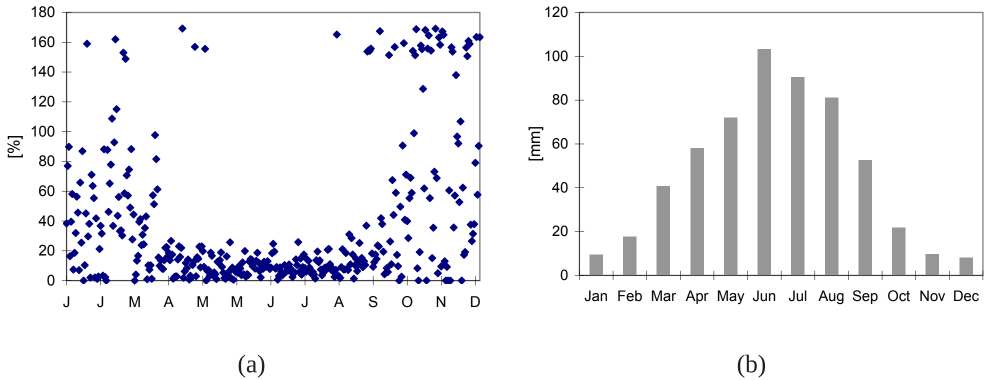

Fig. 9. Monthly ET and daily spatial variation of ET.

HESSD
8, 7055–7090, 2011

Topographic effects on spatial ET and soil moisture

M. Liu et al.

Title Page
Abstract Introduction
Conclusions References
Tables Figures
◄ ►
◄ ►
Back Close
Full Screen / Esc
Printer-friendly Version
Interactive Discussion